Emittance Growth Due to Dipole Ripple and Sextupole

H.-J. Shih, J.A. Ellison, M.J. Syphers, and B.S. Newberger
Superconducting Super Collider Laboratory*
Dallas, TX 75237

Abstract

Ripple in the power supplies for storage ring magnets can have adverse effects on the circulating beams: orbit distortion and emittance growth from dipole ripple, tune modulation and dynamic aperture reduction from quadrupole ripple, etc. In this paper, we study the effects of ripple in the horizontal bending field of the SSC in the presence of nonlinearity, in particular, the growth in beam emittance.

I. INTRODUCTION

For simplicity, we will assume that dipole ripple is localized, i.e., it affects only one dipole magnet. An element-by-element tracking simulation using the program ZTRACK[1] with a localized dipole ripple yields the results shown in Figure 1. In the simulation, 192 particles are tracked, the ripple has a frequency of 743.29 Hz and an amplitude of 10 Gauss, the nominal bending field is 6.684×10^4 Gauss, and the horizontal betatron tune is 123.7821548. Note that the revolution frequency at the SSC is 3441 Hz. We observe from Figure 1 that dipole ripple causes the beam emittance to oscillate between the initial value (3.0×10^{-10} m) and a much larger value ($\approx 2.5 \times 10^{-7}$ m), and that this oscillation is damped with emittance leveling off around an intermediate value ($\approx 1.0 \times 10^{-7}$ m). The beam emittance here is defined as the emittance averaged over the whole beam. Thus it appears that dipole ripple causes the beam to go from one equilibrium state to another where the beam has a larger emittance. In this simulation, we have chosen the ripple frequency to be close to the betatron frequency of 748.62 Hz ($\approx 3441 \times .21785$) and a large ripple amplitude so that we can observe the final equilibrium state in a short time.

One can easily imagine the physics possibly at work here: dipole ripple causes the whole beam to wobble around the design orbit, and nonlinearity, which is built in the full lattice and results in betatron tune dependent on betatron amplitude, then smears the whole beam over a larger phase space area. Our motivation for this work is to understand this quantitatively. In particular, we want to explain the following regarding the beam emittance: the existence of an apparent equilibrium, the amplitude and period of initial oscillations, the final equilibrium value, and how much time it takes to reach the final equilibrium state. To this end, we have constructed a theoretical model using a second-order perturbation theory and the method of averaging. Since the nonlinearity, which is present in the full lattice simulation above, was found to produce a quadratic dependence of betatron tune on betatron amplitude, we represent it in our model by a single sextupole. Our theoretical calculations are in excellent agreement with results from the simple tracking simulations using a linear lattice plus kicks from a single sextupole and a localized dipole ripple.

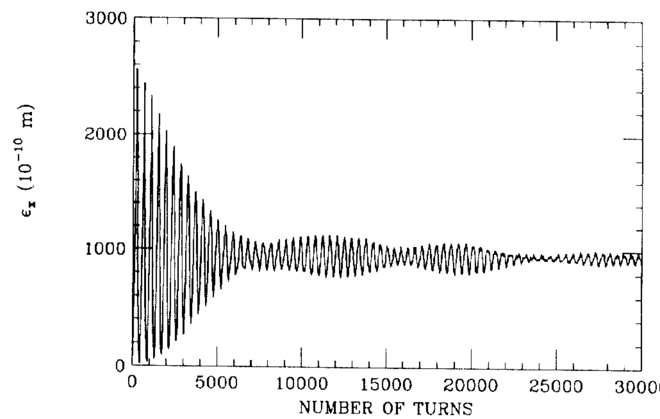

Figure 1. Variation of beam emittance in time from a full lattice simulation.

II. THEORETICAL MODELS

The perturbed beam dynamics is described by the Hamiltonian

$$H(x, x', s) = H_0(x, x', s) + \epsilon H_1(x, s) \tag{1}$$

where $H_0 = \frac{1}{2}(x'^2 + K(s)x^2)$. Here s is the path length along the design orbit, x the horizontal coordinate, $x' = dx/ds$, $K(s)$ the focusing or defocusing function, and ϵ the smallness parameter of the perturbation. For perturbation from a single sextupole and a localized dipole ripple, we have

$$\begin{aligned} \epsilon H_1(x,s) &= \frac{1}{6}S(s)x^3 - F(s)x & (2)\\ S(s) &= S_0\delta_p(s-s_1) & (3)\\ F(s) &= A_0\cos(\omega_r\tau + \phi_r)\delta_p(s-s_0) & (4) \end{aligned}$$

where S_0 is the sextupole strength, δp is the periodic Dirac delta function, s_1 the position of the sextupole, $A_0 = (B_r/B_0)\theta_0$, B_r the ripple amplitude, B_0 the nominal bending field, θ_0 the nominal bending angle, ω_r the angular ripple frequency, τ the time, and s_0 the position of the localized dipole ripple.

To explain initial periodic oscillations, we will consider only the dipole ripple perturbation. Using the independent variable $t = \int ds\big(\nu\beta(s)\big)^{-1}$ and the dependent variable $\eta = x/\sqrt{\beta(s)}$ where $\beta(s)$ is the betatron function, and ν the betatron tune, the equation of motion becomes

$$\frac{d^2\eta}{dt^2} + \nu^2\eta = \nu\beta_0^{\frac{1}{2}}A_0\cos(Q_r t + \theta_r)\delta p(t - t_0) \tag{5}$$

where $Q_r = \omega_r/\omega_0$, ω_0 is the revolution frequency, and β_0 the betatron function at the dipole ripple. Since the right-hand side of (5) can be expressed in the form

$$\sum_{n=-\infty}^{\infty}(A_n e^{i(n+Q_r)t} + B_n e^{-i(n+Q_r)t}),$$

*Operated by the Universities Research Association, Inc., for the U.S. Department of Energy under Contract No. DE-AC35-89ER40486.

[1] L. Schachinger and Y. Yan, SSCL Report SSCL-N-664, September, 1989.

0-7803-1203-1/93$03.00 © 1993 IEEE

we seek a particular solution of the same form. The particular solution we find can be written as

$$\eta_p = \left(\frac{\nu}{2\pi}\right)\beta_0^{\frac{1}{2}} A_0 \sum_{n=-\infty}^{\infty} \frac{\cos\left((n+Q_r)t - nt_0 + \theta_r\right)}{\nu^2 - (n+Q_r)^2}. \qquad (6)$$

With initial conditions $\eta(0) = \eta_0$ and $\xi(0) = \xi_0$, where $\xi = d\eta/dt$, the solution to (5) is then given by

$$\eta = \left(\eta_0 - \eta_p(0)\right)\cos\nu t + \left(\xi_0 - \xi_p(0)\right)\sin\nu t + \eta_p(t). \qquad (7)$$

The results on beam emittance calculated using (7) with $B_r = .322$ Gauss and $\omega_r = (2\pi)(743.29)$ rad sec^{-1} are shown in Figure 2 by a solid curve, which agrees well with results from a full lattice simulation indicated by circles. The crosses are results from a simple tracking simulation, to be described in Section III.

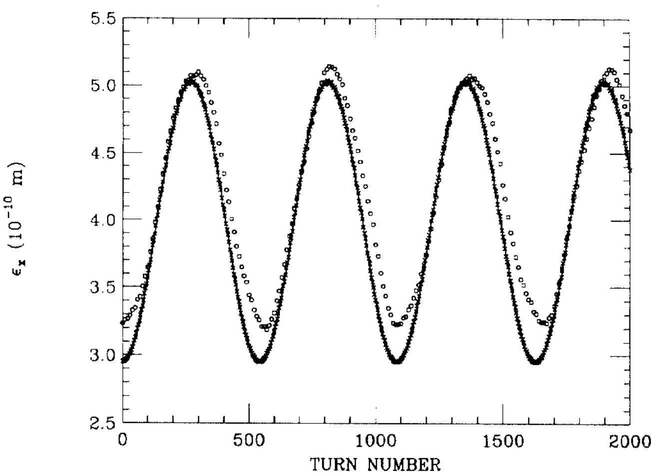

Figure 2. Variation of beam emittance in time. Curve: exact theory; circles: full lattice tracking; crosses: simple tracking.

To explain the final equilibrium state, we will consider both dipole ripple and sextupole perturbations. We will carry out the second-order perturbation calculation in the action-angle representation. The action-angle variables J and ϕ are defined through the following transformation

$$\eta = \left(\frac{2J}{\nu}\right)^{\frac{1}{2}}\cos\phi, \qquad \xi = -(2J\nu)^{\frac{1}{2}}\sin\phi. \qquad (8)$$

The new Hamiltonian for the action-angle variables is given by

$$\mathcal{H}(J,\phi,t) = \nu J + \epsilon\nu^2\beta(s)H_1\left(\beta^{\frac{1}{2}}(s)\left(\frac{2J}{\nu}\right)^{\frac{1}{2}}\cos\phi, s\right). \qquad (9)$$

Here s is understood to be a function of t. From (9) one obtains the Hamiltonian equations of motion

$$\dot{J} = \epsilon f(J,\phi,t), \qquad \dot{\phi} = \nu + \epsilon g(J,\phi,t). \qquad (10)$$

To find approximate solutions of (10) with initial conditions $J(0) = J_0$ and $\phi(0) = \phi_0$, we look for a special autonomous system given by

$$\begin{aligned} \dot{I} &= \epsilon F_1(I) + \epsilon^2 F_2(I) & (11)\\ \dot{\theta} &= \nu + \epsilon G_1(I) + \epsilon^2 G_2(I) & (12) \end{aligned}$$

with initial conditions $I(0) = J_0 + \epsilon u(J_0,\phi_0)$, $\theta(0) = \phi_0 + \epsilon v(J_0,\phi_0)$, and a near identity transformation

$$\begin{aligned} \hat{J} &= I + \epsilon P_1(I,\theta,t) + \epsilon^2 P_2(I,\theta,t) & (13)\\ \hat{\phi} &= \theta + \epsilon Q_1(I,\theta,t) + \epsilon^2 Q_2(I,\theta,t) & (14) \end{aligned}$$

such that $\hat{J}$ and $\hat{\phi}$ satisfy (10) to $O(\epsilon^3)$ with initial conditions $\hat{J}(0) = J_0 + O(\epsilon^2)$ and $\hat{\phi}(0) = \phi_0 + O(\epsilon^2)$. It can be shown that $\hat{J}(t)$ and $\hat{\phi}(t)$ approximate $J(t)$ and $\phi(t)$ to an accuracy of $O(\epsilon^2)$ over a time interval of $O\left(\frac{1}{\epsilon}\right)$. Thus the task of finding solutions to (10) is then reduced to that of finding F_1, F_2, G_1, G_2, P_1, and Q_1. (We don't need to find P_2 and Q_2 if we are concerned with an $O(\epsilon^2)$ accuracy.) Because f and g are periodic in ϕ and quasi-periodic in t, (two periods are involved: one is associated with the beam revolution and the other associated with ripple) we require that P_1, P_2, Q_1 and Q_2 are also periodic in θ and quasi-periodic in t.

For dipole ripple and sextupole perturbations, one can write $f = f^{(r)} + f^{(s)}$ and $g = g^{(r)} + g^{(s)}$ where the superscripts (r) and (s) stand for contributions from dipole ripple and sextupole respectively. A lengthy calculation involving expansion in ϵ to the second order and averaging over θ and t yields $F_1 = 0$, $G_1 = 0$, $F_2 = 0$, $G_2 = G_2^{(s)} = \langle g_I^{(s)}P_1^{(s)} + g_\theta^{(s)}Q_1^{(s)}\rangle$ where $\langle\rangle$ denotes the average over θ and t, the subscripts I and θ denote the derivatives with respect to I and θ respectively, and $P_1^{(i)}$ and $Q_1^{(i)}$ $(i = r, s)$ satisfy the homological equations $P_{1t}^{(i)} + \nu P_{1\theta}^{(i)} = f^{(i)}$ and $Q_{1t}^{(i)} + \nu Q_{1\theta}^{(i)} = g^{(i)}$ respectively. We refer the readers to the paper by H. Dumas et al.[2] for more information on our averaging procedure. In summary, our approximate solutions $\hat{J}$ and $\hat{\phi}$ are given by

$$\begin{aligned} \dot{I} &= 0, \qquad \dot{\theta} = \nu + \epsilon^2 G_2^{(s)}(I) & (15)\\ \hat{J} &= I + \epsilon\left(P_1^{(r)}(I,\theta,t) + P_1^{(s)}(I,\theta,t)\right) & (16)\\ \hat{\phi} &= \theta + \epsilon\left(Q_1^{(r)}(I,\theta,t) + Q_1^{(s)}(I,\theta,t)\right) & (17) \end{aligned}$$

with $u(J,\phi) = -P_1(J,\phi,0)$, $v(J,\phi) = -Q_1(J,\phi,0)$, and $G_2^{(s)}$, $P_1^{(s)}$, $Q_1^{(s)}$, $P_1^{(r)}$ and $Q_1^{(r)}$ given by

$$G_2^{(s)}(I) = \frac{3}{64\pi^2} I\beta_1^5 S_0^2 \times \left\{-\frac{10}{9} + \nu\left(\psi(1+\nu) - \psi(1-\nu) + \frac{\psi(1+3\nu) - \psi(1-3\nu)}{3}\right)\right\} \qquad (18)$$

$$P_1^{(s)}(I,\theta,t) = -\left(\frac{\nu}{32}\right)^{\frac{1}{2}} I^{\frac{3}{2}}\beta_1^{\frac{5}{2}} S_0 \times \left\{\frac{\cos\left(\nu([t_1'] - \pi) - \theta\right)}{\sin(\pi\nu)} + \frac{\cos\left(3\nu([t_1'] - \pi) - 3\theta\right)}{\sin(3\pi\nu)}\right\} \qquad (19)$$

$$Q_1^{(s)}(I,\theta,t) = -\left(\frac{\nu}{128}\right)^{\frac{1}{2}} I^{\frac{1}{2}}\beta_1^{\frac{5}{2}} S_0 \times \left\{3\frac{\sin\left(\nu([t_1'] - \pi) - \theta\right)}{\sin(\pi\nu)} + \frac{\sin\left(3\nu([t_1'] - \pi) - 3\theta\right)}{\sin(3\pi\nu)}\right\} \qquad (20)$$

$$P_1^{(r)}(I,\theta,t) = \left(\frac{\nu}{8}\right)^{\frac{1}{2}} I^{\frac{1}{2}}\beta_0^{\frac{1}{2}} A_0 \times \left\{\frac{\cos\left((\nu - Q_r)([t_0'] - \pi) - (\theta - Q_r t - \theta_r)\right)}{\sin\pi(\nu - Q_r)} + \frac{\cos\left((\nu + Q_r)([t_0'] - \pi) - (\theta + Q_r t + \theta_r)\right)}{\sin\pi(\nu + Q_r)}\right\} \qquad (21)$$

[2] H.S. Dumas, J.A. Ellison and A.W. Sánez, *Annals of Physics* **209**, 97 (1991).

$$Q_1^{(r)}(I,\theta,t) = \left(\frac{\nu}{32}\right)^{\frac{1}{2}} I^{-\frac{1}{2}}\beta_0^{\frac{1}{2}}A_0 \times \left\{ \frac{\sin\left((\nu - Q_r)([t_0'] - \pi) - (\theta - Q_r t - \theta_r)\right)}{\sin\pi(\nu - Q_r)} + \frac{\sin\left((\nu + Q_r)([t_0'] - \pi) - (\theta + Q_r t + \theta_r)\right)}{\sin\pi(\nu + Q_r)} \right\} \quad (22)$$

where $\psi(x) \equiv \Gamma'(x)/\Gamma(x)$, β_1 is the betatron function at the sextupole, $t_0' \equiv t - t_0$, $t_1' \equiv t - t_1$, and [ ] denotes the modulus between 0 and 2π. Our perturbation calculations indicate that, up to the second order, dipole ripple contributes only in the near-identity transformations (16) and (17). The vector field, (15), is still given by sextupole perturbation.

Figure 3 shows the phase space distribution of a beam after 50000 turns calculated using (15)–(22). The beam consists of 500 particles and is initially uniformly distributed in the ranges of $0.1 < x < 0.3$ mm and $-2.4 < x' < -2.0$ μrad. In this calculation, the ripple has a frequency of 720 Hz and an amplitude of 0.322 Gauss, and the sextupole strength is $S_0 = -0.55580$, which reproduces the relationship $G_2^{(s)} = (1.0567 \times 10^3)I$ obtained from a fit to the dependence of betatron tune on betatron amplitude in the full lattice mentioned in Section I. For an initial beam whose distributions in x and x' are Gaussian (and thus the distribution in the angle variable is uniform in the linear approximation), the averages of the second order terms over the angle variable are zero, and one has to go to a third-order perturbation calculation. However, a serious drawback of the action-angle approach is that $\epsilon P_1^{(r)}/I$ is proportional to $I^{-\frac{1}{2}}$, and the perturbation calculation breaks down for small I. We are now working on a new set of variables which doesn't have this problem.

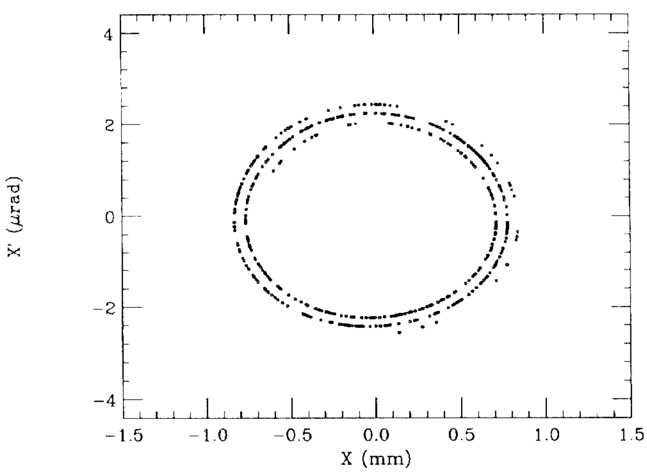

Figure 3. Phase space distribution of a beam after 50000 turns from a perturbation calculation.

III. TRACKING SIMULATIONS

To check our theoretical models, we have tracked particles using linear transfer matrices with kicks from a single sextupole and a localized dipole ripple. This simple tracking method has produced the results indicated by crosses in Figure 2, and reproduced those shown in Figure 3. It also gives results very similar to those shown in Figure 1. The results from a run following 500 particles with $B_r = 1$ Gauss, $\omega_r = 2\pi(720)$ rad sec^{-1}, and $\nu = 123.78677$ is shown in Figure 4. Because the computing time with the simple tracking simulation is greatly reduced, we can now more easily determine the dependence of the final equilibrium emittance on a few relevant parameters, e.g., ripple amplitude. Figure 5 summarizes our study on the dependence of relative emittance growth on ripple amplitude and betatron tune. The ripple frequency is fixed at 720 Hz.

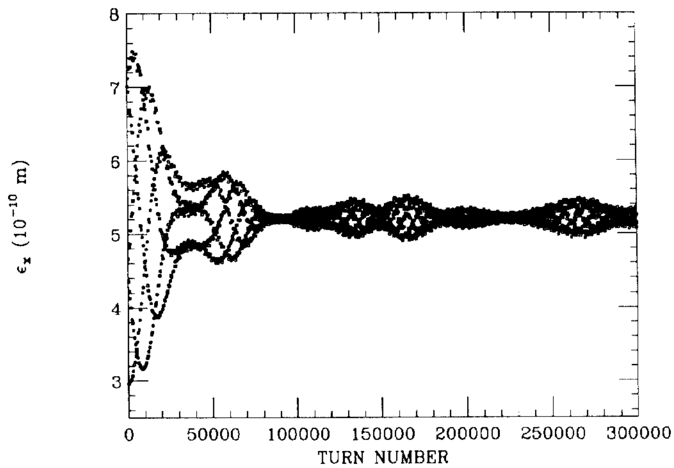

Figure 4. Variation of beam emittance in time from a simple tracking simulation.

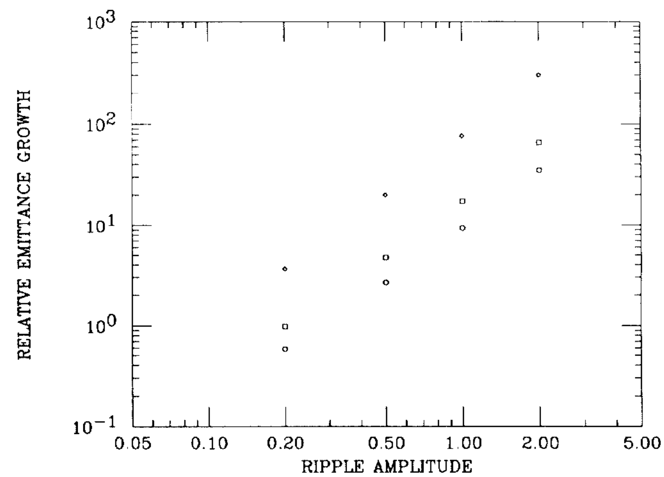

Figure 5. Relative growth in beam emittance as a function of ripple amplitude. Circles: $\nu = 123.77877$; squares: $\nu = 123.78215$; diamonds: $\nu = 123.78677$.

IV. CONCLUSIONS

Theoretical models have been developed to explain the features of emittance evolution observed from the full lattice simulation in the presence of dipole ripple. Our calculation with just dipole ripple is exact and explains the observed initial oscillations of beam emittance. Our model for the apparent existence of final equilibrium state is based on a second-order perturbation calculation involving both dipole ripple and sextupole. Its predictions agree very well with results from simple tracking simulations using a linear lattice plus kicks from dipole ripple and sextupole. The simple tracking method that we have developed is very fast and very suitable for exploring final equilibrium states by changing relevant parameters over a wide range.

J.A.E. gratefully acknowledges discussions with M. Kummer.